

Journal of Engineering Sciences and Innovation

Volume 10, Issue 1 / 2025, pp. 21 -32 http://doi.org/10.56958/jesi.2025.10.1.21

C. Chemical Engineering, Materials Science and Engineering

Received 10 October 2024
Received in revised form 9 December 2024

Accepted 10 March 2025

Microstructures of novel Al-containing Co-based and Ni-based alloys designed to be reinforced by TaC carbides

PATRICE BERTHOD^{1,2*}

¹Faculté des Sciences et Technologies, Université de Lorraine, France ²Institut Jean Lamour, Université de Lorraine, 2 allée André Guinier, 54000 Nancy, France

Abstract. Chromium and aluminum are the principal elements to protect superalloys by the development of an efficient continuous external oxide scale. Aluminum is used in γ/γ single–crystals while chromium is chosen in carbide–strengthened alloys. In this work it was attempted to totally replace chromium by aluminum in model Co–based and Ni–based superalloys designed to contain TaC as reinforcing particles. The consequences on the ascast microstructures were investigated by electron microscopy and first mechanical results at room temperature were obtained by hardness measurement. Removing chromium and introducing aluminum did not obstruct the appearance of TaC carbides which precipitated in rather important quantity, in the interdendritic spaces and with the script–like morphology, similarly to the original equivalent alloys containing chromium. The most noticeable microstructure change was observed for the Co–based alloys with 10 wt.% Al since almost a half of the matrix was a new phase very rich in Al, probably an intermetallic phase close to Co_3Al . Its presence is possibly the reason of the increase in hardness of this alloy.

Keywords: Cobalt alloy, Nickel alloy, Aluminum, TaC carbides, Microstructures.

1. Introduction

Carbides—strengthened superalloys were among the earliest metallic alloys to appear for answering the needs of mechanically strong and corrosion—resistant materials for long time working at high temperature in the first jet engines [1]. With the progress of the clean elaboration means (e.g. controlled/inert atmospheres [2]) and the development of microstructures involving reactive elements (i.e. solid solution strengthening by heavy atoms, intermetallic precipitates [3]), the reinforcement by carbides was more or less hindered by novel reinforcing solutions

 ${\rm *Correspondence\ address:\ patrice.berthod@univ-lorraine.fr}$

exploited in the modern superalloys (particularly the γ/γ 'single crystalline alloys and oxide dispersion strengthened (ODS) alloys). However the hardening of superalloys by primary eutectic carbides and/or by finely dispersed secondary carbides is still a solution which keeps advantages. For instance, when high chromium contents are required to resist hot corrosion by some aggressive molten substances (particular compositions of CMAS, of molten salts, of molten glass...) [4], the intermetallic gamma prime precipitates cannot be present in alloy with volume fractions as high as the almost 70% existing in single-crystals. Furthermore, some carbides of the MC stoichiometry succeed in remaining, at 1100°C and more, in alloy with still volume fraction high enough while gamma prime tend to totally disappear at so elevated temperatures. Such MC carbides can be encountered in the MarM-509 Co-based superalloy but also in Ni-based superalloys [6, 7], even directionally solidified [8] or single-crystalline [9]. Generally rather stable at high temperature (more than chromium carbides), they may evolve/decompose with time, in Ni-based superalloys [10-12] as well as in Co-based superalloys [13]. MC carbides can be of different types – TaC, NbC, HfC or ZrC in a Co-based alloys [14] for instance, but they are often tantalum monocarbides (e.g. [15,16]). Despite that they are generally less stable at high temperature, the chromium carbides, of the M₇C₃ type notably, can compete with some MC (TiC, NbC or TaC for instance) in some matrix environments (e.g. Nibased, more than in Co-based or Fe-based), when Cr is present in rather proportions (e.g. 20 to 30 wt.%). Since Al is not able to form carbides as stable as chromium carbides, it is possible that choosing Al instead Cr in alloys designed to be strengthened by MC carbides and destined to applications involving only exposure to hot air and not contact with aggressive melts, represent a good solution to preserve the MC carbides from competition with other carbides, during solidification as well as during use at high temperature.

In this work it is wished to observe the persistence, during solidification, of TaC carbides in Co–Al and Ni–Al matrix environments with three selected conventionally cast alloys all containing 0.4 wt.% C and 6 wt.% Ta (for equality of the molar contents of Ta and C): two cobalt–based ones (containing 5 or 10 wt.% Al) and a nickel–based one (containing 5 wt.%). The obtained as–cast microstructures will be specified as well as the hardness of these alloys.

2. Methodology

First, the three alloys were elaborated through a foundry way, involving techniques classically used for superalloys: high frequency induction melting and solidification in an inert atmosphere. Each alloy was prepared from pure elements (Alfa Aesar, purity better than 99.5 wt.%). Blocky parts of Co or Ni, and of Cr, flakes of Ta and rods of graphite were accurately weighed using a precision balance, targeting the Co–5 Al or 10 Al–0.4 C–6 Ta and Ni–5 Al–0.4 C–6 Ta compositions in weight percent. They were placed in the copper crucible belonging to the high frequency induction furnace (CELES, France). The Melting chamber

was closed by placing a silica tube separating the crucible (inside) and the induction copper coil surrounding the crucible (outside). After the {pumping \rightarrow primary vacuum, introduction of pure Ar} sequences repeated three times, the internal gaseous environment was of about 300 millibars of pure argon. The generator produced an alternative current (100 kHz for frequency, 5kV for voltage) which increased progressively. This induced Foucault's currents which heated, by Joule effect, the external faces of the metallic parts. After about 2 minutes all metals were melted and the liquid alloy was maintained at high temperature during about ten minutes to be sure that the chemical homogenization was achieved. By decreasing power, the liquid alloy cooled, solidified and cooled in the solid state.

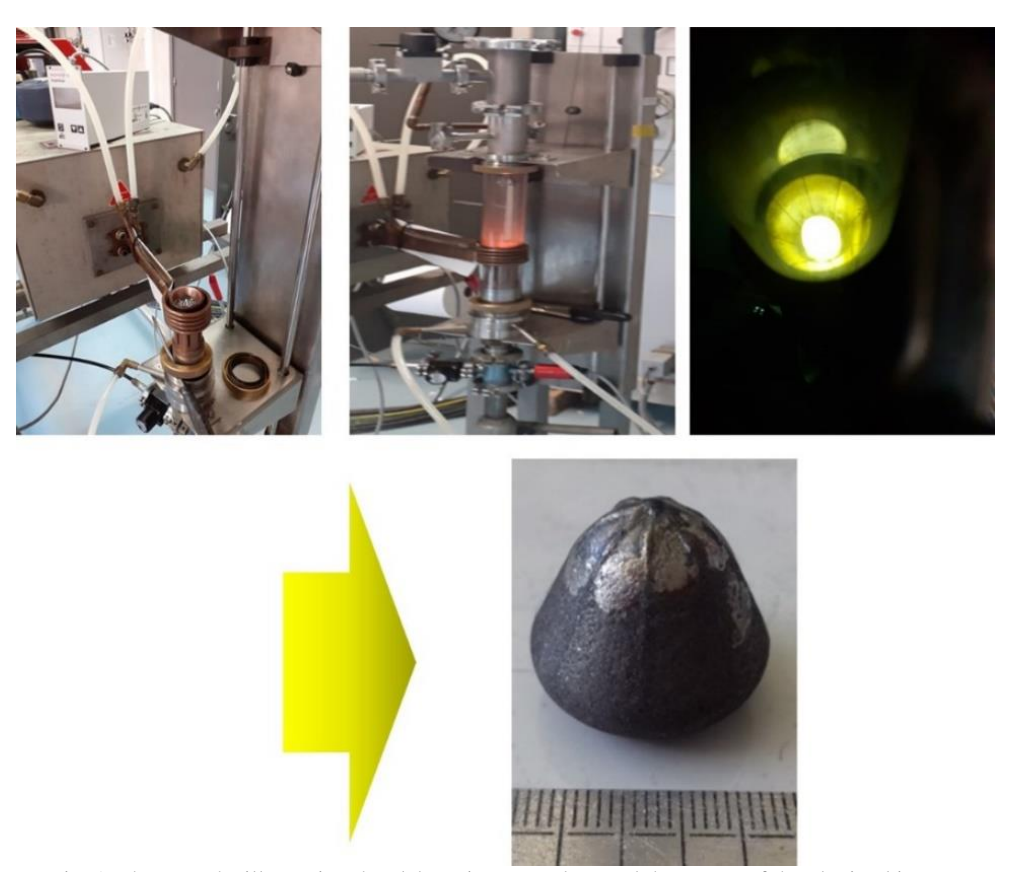


Fig. 1. Photographs illustrating the elaboration procedure and the aspect of the obtained ingots.

Second, the obtained ovoid ingots – all weighing about 40 grams – were immersed in a molten cold {resin + hardener} mixture. Resin rigidification took about four hours, at the end of which extraction out of the plastic mold was done. The embedded ingots were cut using a precision metallographic saw, operation become much easier on a cylindrical embedded ingot. This allowed obtaining two samples for a same alloy. One of them was ground using SiC papers from 240 grade to

1200 grade, then polished using a textile disks enriched in micrometric alumina particles. The obtained mirror–like sample was then available for microstructure examinations and indentation tests. The microstructures were characterized by observation at several magnifications using a Scanning Electron Microscope (SEM; mode: back scattered electrons imaging, BSE) and by chemical analysis using Energy Dispersion Spectrometry analysis (EDS). The SEM was a JEOL JSM-6010LA one. Indentations were carried out according to the Vickers method using a Testwell Wolpert machine, under a load equal to 30kg. Per alloy, five indentations were performed, leading to an average value and a standard deviation value.

3. Results and discussion

Chemical compositions of the three alloys

The chemical composition measured by three full frame EDS analyses on each metallographic sample containing the as—cast part of the alloy evidenced that the targeted composition was globally obtained (Table 1).

Table 1.	Chemica	al composi	tions	of the	obtai	ned al	loy	S
(average and	standard	deviation	from	three	×250	areas.	in	wt.9

Wt.%	Ni	Co	Al	Ta	C
Ni5	basa	/	4.2	7.6	0.4 (targeted)
INIS	base	/	±0.1	±0.7	0.4 (targeted)
Co5	,	hogo	4.1	8.0	0.4 (tamastad)
C03	/	base	±0.2	±0.4	0.4 (targeted)
Co.10	,	hogo	8.4	5.2	0.4 (tamastad)
Co10	/	base	±0.1	±0.5	0.4 (targeted)

Microstructure of the Ni5 alloy

The microstructure of Ni5 is illustrated at different scales in Figure 2, from a very general view (×250) to a much more detailed view (×1000). The alloys seems to be double–phased. It contains a matrix which is dendritic and of two levels of gray: clear in majority but darker close to the script–like carbides. These carbides, much brighter than the matrix, are located in the interdendritic areas where they formed a eutectic compound with the darkest part of the matrix. Elemental mapping was performed with the SEM and its EDS device on an area in the Ni5 alloy, for two magnifications (Figure 3). Aluminum seems homogeneously distributed in the matrix. The results show that the bright carbides are tantalum carbides and they are surrounded by a dark part of matrix with which they form the eutectic compound. Obviously this darkness of this eutectic part of the matrix is principally due to a relative poorness in tantalum.

A series of EDS spot analyses were performed in the bright phase, in the peripherical dark part of matrix mixed with the bright carbides and in the clear part of the matrix. Results are available in Table 2.

Table 2. Chemical composition of the two zones of the matrix of the Ni5 alloy (average and standard deviation from five results of the spot analyses performed at $\times 1000$, in wt.%)

Wt.%	Ni	Al	Ta	localization
Dright part of matrix	balance	4.3	5.2	Core of
Bright part of matrix	balance	±0.1	±0.2	dendrites
Doult most of mothin	halamaa	4.5	2.7	Areas mixed
Dark part of matrix	balance	±0.1	±0.3	with TaC

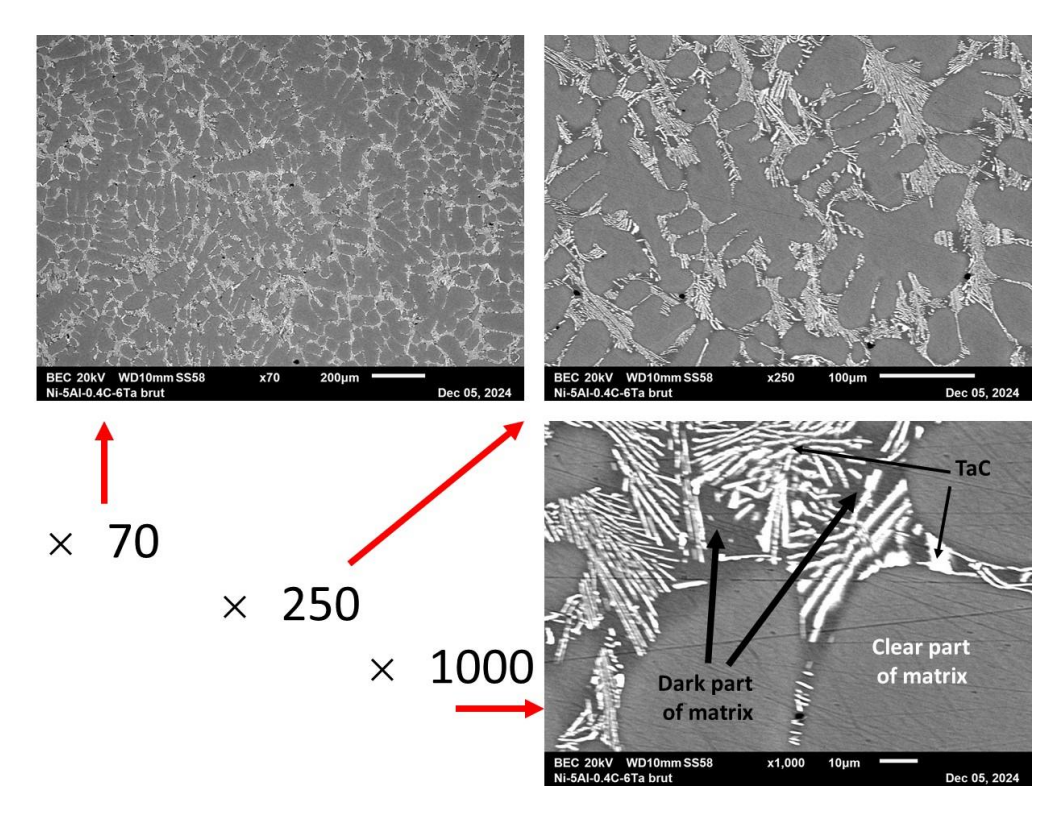


Fig. 2. General or detailed views of the microstructure of the Ni5 alloy (SEM, BSE mode of imaging).

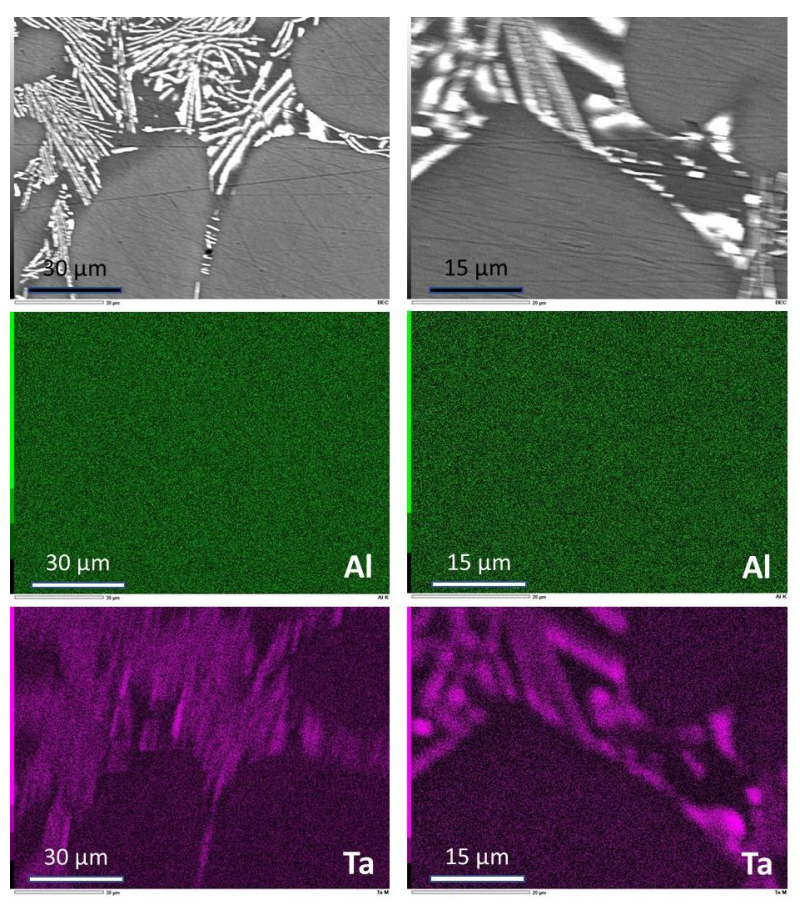


Fig. 3. Elemental EDS maps acquired on Ni5 and their SEM/BSE micrographs of the analyzed areas (left: ×1000, right: ×2000); only for Al and Ta (Ni and C not represented).

These quantitative results confirm that the content in Al is seemingly the same everywhere in the matrix and also that the dark part of matrix (close to the carbides) contains two times less tantalum than the clear part. This explains the difference of gray level observed in BSE imaging (the molar mass of tantalum is almost four times the one of nickel). The spot analyses performed in the bright phases also confirm that these particles are carbides (high concentrations in tantalum and in carbon). Due to the small size of these carbides the interaction peer also affect matrix. Furthermore C is a too light element to be accurately rated by EDS, even this is more efficient in particles very rich in carbon such as the present carbides. Consequently it is not really possible to assess the Ta and C contents in these particles. Nevertheless one can consider as very probable that these bright particles are TaC carbides.

Microstructure of the Co5 and Co10 alloys

The microstructure of Co5 is also illustrated at different scales, in Figure 4. This second alloy, based on cobalt and designed to contain the same aluminum, tantalum and carbon as Ni5, is rather different. It is also double—phased and constituted of a dendritic matrix and of a eutectic compound mixing script—like Ta—rich particles and the peripherical part of the dendrites, but the eutectic compound is significantly more extended. Consequently the matrix appears as less present than in Ni5.

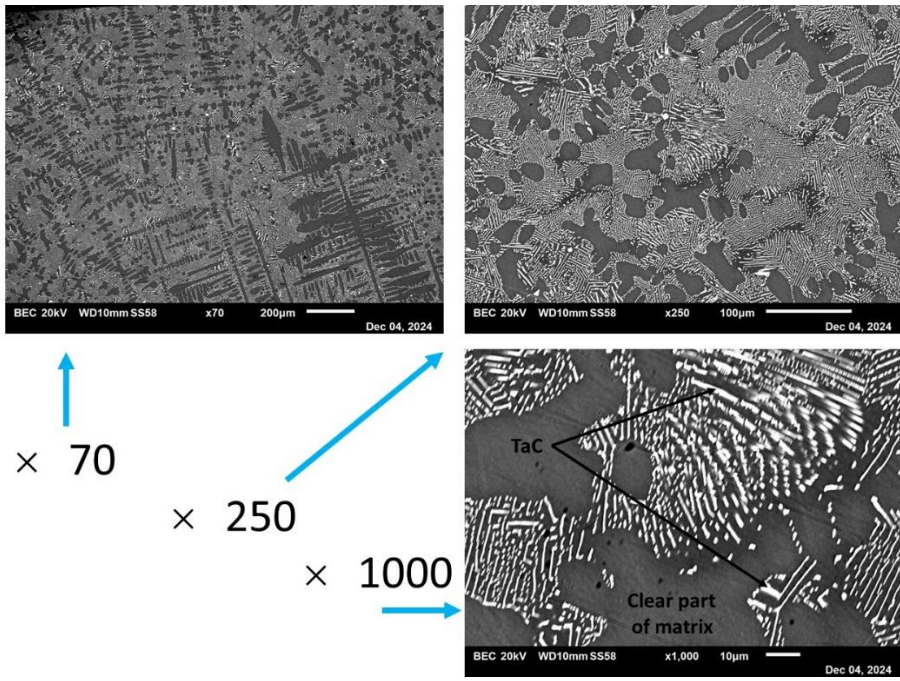


Fig. 4. General or detailed views of the microstructure of the Co5 alloy (SEM, BSE mode of imaging).

The elemental EDS maps (Figure 5) suggests here too that the bright particles are very rich in tantalum and also in C in the rare coarse blocky carbides existing in addition the eutectic ones. The part of matrix surrounding the Ta–rich particles are here too darker than in the dendrites' cores but it is seemingly due to a higher Al content than everywhere else in the matrix, and not to a lower Ta content.

EDS spot analyses were here too performed in the bright particles and in the dendrites (results in Table 3). The bright particles are again tantalum carbides, probably TaC carbides (spot analyses performed on particularly coarse blocky bright particles led to contents in C and in Ta rather close to one another). The matrix, which contains about the same Al content as in the Ni5 alloy (4.1 wt.% Al against 4.3 in Ni5 matrix), is obviously poorer in Ta than the matrix of the later alloy: 2.3 wt.% Ta against 5.2 in Ni5. This can explain the more developed TaC

network in Co5 than in Ni5. Logically more carbon ought to be present in solid solution in the Ni5 matrix than in the Co5 one.

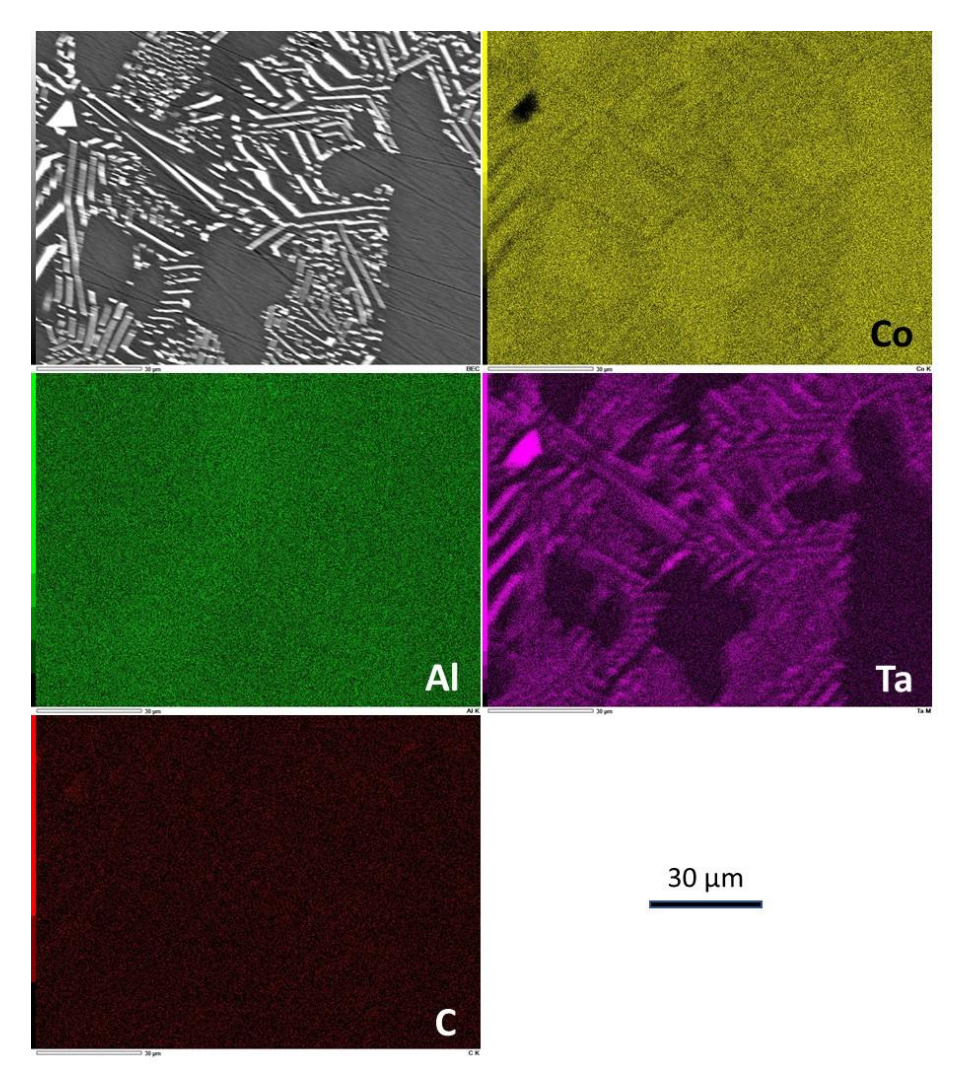


Fig. 5. Elemental EDS maps acquired on Co5 and their SEM/BSE micrograph of the analyzed area (magnification: ×1000).

The microstructure of the Co10 alloy is illustrated in Figure 6, an elemental EDS map is presented in Figure 7 and results of spot analyses performed in each phase are gathered in Table 4. This microstructure is quite different from the two preceding ones, for two reasons. First the blocky tantalum carbides (rich in Ta and in C according the EDS map) are much more numerous and the eutectic carbides much less developed. Second the matrix seems composed of two distinct phases, one (darker, 11.6 wt.% Al) richer in Al than the other (clear, 6.4-6.9 wt.% Al). Furthermore, the additional presence of small clear areas in the dark matrix part

leads to think to another eutectic compound, formed of these two parts of the matrix. When one consider the atomic composition of the dark part of matrix (about 77.0 at.% Co, 22.4 at.% Al, 0.6 at.%Ta) this phase seems close to the intermetallic Co₃(Al,Ta).

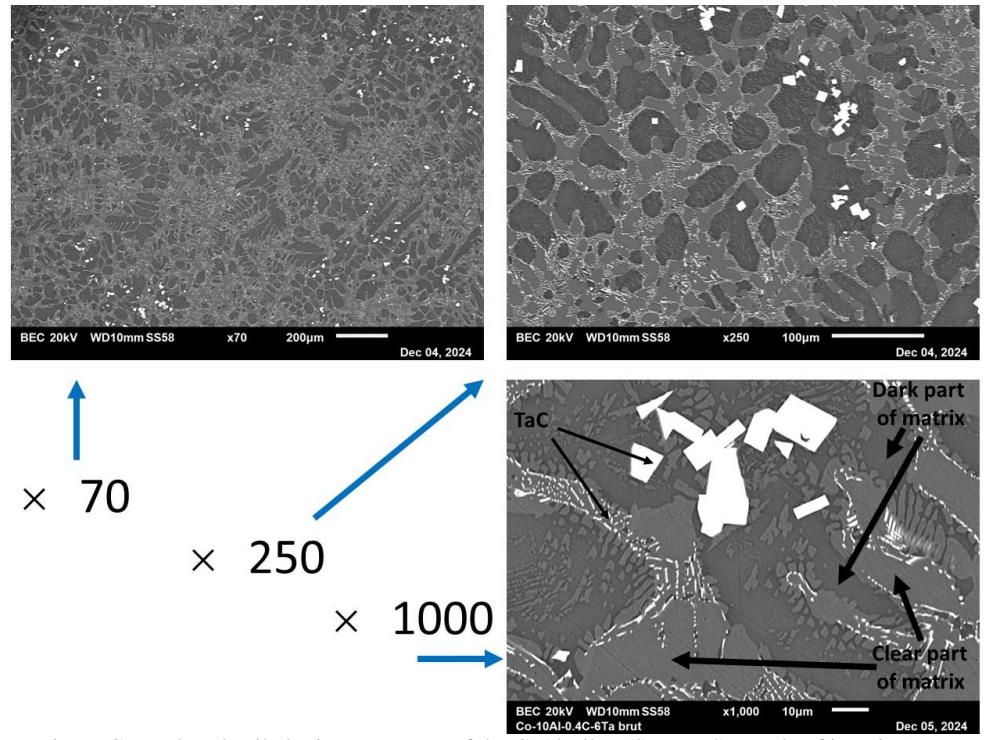


Fig. 6. General or detailed microstructures of the Co10 alloy (SEM, BSE mode of imaging).

Table 3. Chemical composition of the matrix of the Co5 and Co10 alloys (average and standard deviation from five results of the spot analyses performed at ×1000, in wt.%)

Wt.%	Co	Al	Ta	Gray level in BSE
Co5 matrix	balance	4.1 ±0.1	2.3 ±0.1	clear

Table 4. Chemical composition of the matrix of the Co5 and Co10 alloys (average and standard deviation from five results of the spot analyses performed at $\times 1000$, in wt.%)

Wt.%	Co	Al	Ta	Gray level in BSE
Co10: clear matrix	balance	6.9	2.0	clear
Coro. cicai matrix	barance	± 0.1	±0.3	Cicai
Co10: clear areas inserted in	balance	6.4	1.5	clear
the dark part of matrix	balance	±0.3	±0.2	Clear
Colly dork part of matrix	balanaa	11.6	2.2	dark
Co10: dark part of matrix	balance	±0.4	±0.3	uark

Table 5. Atomic composition of the dark part of the matrix of the Co10 alloys (average and standard deviation from five results of the spot analyses performed at ×1000, in wt.%)

At.%	Co	Al	Ta	Co/(Al+Ta)
Co5 matrix	77.0	22.4	0.6	22
Co5 matrix	±0.7	± 0.8	± 0.1	≈ 3.3

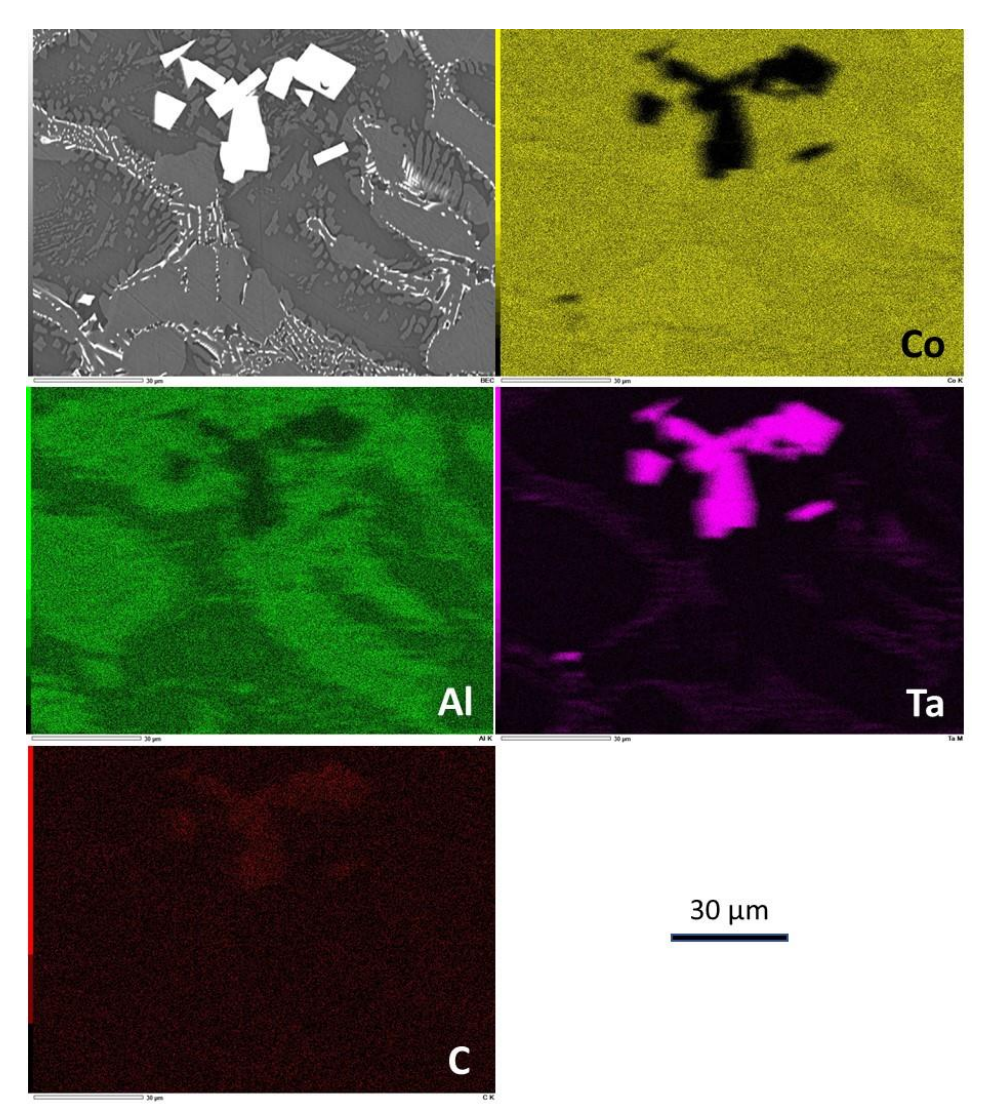


Fig. 7. Elemental EDS maps acquired on Co10 and their SEM/BSE micrograph of the analyzed area (magnification: ×1000).

Vickers hardness of the three alloys

The five indentations performed per alloy under a 30 kg load led to the values presented in Table 6. The average ones are ordered as follows: 344 (Co5) < 376

(Ni5) < 417 (Co10). It seems that the effect of the intermetallic phase rich in Al present in the Co10 alloy overcomes the hardening by TaC carbides (these ones are more present in Co5 than in Co10). The hardness of Ni5 which is higher than the Co5 one appears as questionable: generally a Co–based alloys is harder than a Ni–based one with equivalent second phases, and furthermore Ni5 contains less TaC than Co5. This needs to investigate deeper.

Table 6. Values of hardness obtained for the three alloys according to the Vickers method,

Alloy \ HV _{30kg}	Average	Standard deviation
Ni5	376	6
Co5	344	7
Co10	417	16

4. Conclusion

Obviously, replacing chromium by aluminum in its hot oxidation—resistance role did not forbid the appearance of the same TaC carbides as in the original alloys. On the contrary, these ones precipitated in rather important quantity, in the interdendritic spaces and with the script—like morphology. This is the Co—based alloy with the higher Al addition that presents the most noticeable microstructure change, with the replacement of half of the matrix by a new phase very rich in Al. Possibly responsible of the increase in hardness, this — possibly intermetallic Co₃Al — phase may influence the mechanical behavior of the alloy at high temperature. The high temperature behaviors of these microstructures as well as the creep and oxidation resistances will be soon investigated for these three alloys, after having controlled their refractoriness by thermal analysis. Differences in behavior can be expected for both properties.

References

- [1] Sims C.T., Hagel W.C., The Superalloys-Vital High Temperature Gas Turbine Materials for Aerospace and Industrial Power, John Wiley & Sons, 1972.
- [2] Sims C.T., Stoloff N.S., Hagel W.C., Superalloys II. High Temperature Materials for Aerospace and Industrial Power, John Wiley & Sons, 1987.
- [3] Donachie M.J., Donachie S.J., *Superalloys: A Technical Guide* (2nd edition), ASM International, 2002.
- [4] Kofstad P., High Temperature Corrosion, Elsevier Applied Science, 1988.
- [5] Young D.J., *High Temperature Oxidation and Corrosion of Metals*, Elsevier Corrosion Series, 2008.
- [6] Dong X., Zhang X., Du K., Zhou Y., Jin T., Ye H., Journal of Materials Science and Technology, 28, 1031, 2012.
- [7] Liu L., Sommer F., Scripta Metallurgica et Materialia, 30, 587, 1994.
- [8] Li Q., Tian S., Yu H., Tian N., Su Y., Li Y., Materials Science & Engineering A, 633, 20, 2015.
- [9] Cutler E.R., Wasson A.J., Fuchs G.E., Scripta Materialia, 58, 146, 2008.
- [10] Yang J., Zheng Q., Sun X., Guan H., Hu Z., Materials Science and Engineering A, 429, 341, 2006.
- [11] Lvov G., Levit V.I., Kaufman M.J., Metallurgical and Materials Transactions A, 35A, 1669, 2004.

- [12] Yang J., Zheng Q., Sun X., Journal of Materials Science, 41, 6476, 2006.
- [13] Gui W., Zhang H., Yang M., Jin T., Sun X., Zheng Q., Journal of Alloys and Compounds, 695, 1271, 2017.
- [14] Berthod P., Journal of Alloys and Compounds, 481, 746, 2009.
- [15] Montazeri M., Ghaini F.M., Farnia A., International Journal of Materials Research, 102, 1446, 2011.
- [16] Karge L., Gilles R., Mukherji D., Strunz P., Beran P., Hofmann M., Gavilano J., Keiderling U., Dolotko O., Kriele A., Neubert A., Rösler J., Petry W., *Acta Materialia*, **132**, 354, 2017.